JOURNAL OF MATERIALS SCIENCE 21 (1986) 3783–3800

Ultrasonic relaxation studies of the vitreous system Mo–P–O in the temperature range 4 to 300 K

B. BRIDGE, N. D. PATEL*
Department of Physics, Brunel University, Uxbridge, Middlesex UB8 3PH, UK

A detailed study of ultrasonic relaxation in the entire vitreous range of the glass system MoO_3–P_2O_5 (0 to 83 mol% MoO_3) is presented. Pulse echo techniques were employed in the frequency range 15 to 135 MHz and temperature range 4 to 300 K. Ultrasonic absorption peaks were observed at various temperatures between 74 and 128 K depending upon glass composition and operating frequency. The composition dependence of the position and overall shape of the loss peaks was analysed in terms of an assumed loss of the standard linear solid type, with low dispersion, and a broad distribution of Arrhenius-type relaxation times with temperature-independent relaxation strengths (two-well formalism with a broad distribution of asymmetries). After a brief review of two-well formalism, a simple central force model of the microscopic origins of two-well systems is presented, to demonstrate that (in contrast to what has often been assumed previously) there is no need to postulate bond directionality effects to account for "acoustically active" two-well systems in glassy materials. Also given is a quantitative model of the deformation potential arising in phenomenological models of acoustic loss produced by two-well systems. The shape of the loss peaks (i.e. the shape of the relaxation spectra), and the mean activation energy determined from the frequency dependence of the loss-peak temperature (V_p), are both strongly composition-sensitive. Furthermore, they are found to correlate with the elastic properties of the glass system and the assumed bond force constants. The conclusion thus arrived at is that the acoustic loss is a property of the vitreous network as a whole rather than due to a second-order effect like the presence of dangling bonds or polar groups, or to network holes etc. Finally a microscopic phenomenological model is developed to account for the composition dependence of the observations. In particular, semi-theoretical formulae are used to express V_p and the fractional number of two-well systems per oxygen atom, N, as a function of the bulk modulus and a mean cation–anion stretching force constant. Considerable success was thereby achieved in explaining the contrasting behaviour of V_p and N.

1. Introduction

Peaks in the temperature dependence of acoustic wave absorption in inorganic oxide and halogenide glasses occurring in the range 4 to 300 K have long been attributed to loss mechanisms of the standard linear solid type, with low dispersion (SLSLD) and Arrhenius-type relaxation times. Formally the loss has been ascribed to the presence of particles or groups of particles moving in double-well potentials, and experimental values of activation energy and attempt frequency suggest wells and particle dimensions of atomic orders of magnitude, i.e. we are talking about the motions of single atoms or small groups of atoms. However, little progress has been made towards a quantitative understanding of the loss process in terms of assumed atomic configurations. Our work was commenced on an assumption that a study of how the loss behaviour varies with gradual and wide-ranging changes in glass composition could produce the key to an understanding of the microscopic origins of the loss. Much of the past literature has been focused on the effects of gross compositional changes, though a detailed study of gradual composition changes has been given for borosilicate glass [1]. The following presentation is the first detailed study of two-well systems in a complete phosphate glass system. The results are interpreted in terms of atomic ring sizes and bond force constants. Initially the formal relationships required for our data analysis, widely dispersed in the literature, are collected together, and we then present a central force model of the magnitude of the two-well barrier heights and deformation potential occurring in the phenomenological theory.

2. General theoretical considerations

On thermodynamical grounds alone [2] it can be

Present address: MacMaster University, Department of Metallurgy and Materials Science, 1280 Main Street West, Hamilton, Ontario L85 4L7, Canada.

0022–2461/86 $03.00 + .12 © *1986 Chapman and Hall Ltd.*

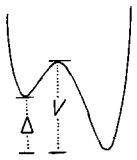

Figure 1 Two-well system with barrier height V and asymmetry Δ.

shown that for a system of n particles per unit volume moving in identical double-well potentials of barrier height V (Fig. 1), the internal friction is

$$Q^{-1} = \frac{2\alpha c}{\omega} = \frac{nD^2}{\varrho c^2}\frac{\mathrm{d}}{\mathrm{d}\Delta}\left(\frac{1}{1+\mathrm{e}^{\Delta/kT}}\right)\frac{\omega\tau}{1+\omega^2\tau^2} \quad (1)$$

where

$$\tau = \tau_0 \mathrm{e}^{V/kT}(1+\mathrm{e}^{-\Delta/kT}) \quad (2)$$

Here k is Boltzmann's constant, T is the absolute temperature, α is the acoustic wave absorption coefficient in nepers per unit length, ω is the angular frequency, c is the phase velocity for $\omega \to 0$, τ is the relaxation time, τ_0^{-1} is the classical vibration frequency (attempt frequency) for the particle in either well, Δ is the free-energy difference between corresponding particle states in the two wells, i.e. the separation of the well minima; and the "deformation potential" D is the energy shift of the two-well states in a strain field of unit strength, averaged over all possible well orientations.

In the case of symmetric wells, or when the asymmetry Δ is such that $\Delta/kT \ll 1$, Equations 1 and 2 simplify to

$$Q^{-1} = \frac{2\alpha c}{\omega} = \frac{nD^2}{4\varrho c^2 kT}\left(\frac{\omega\tau}{1+\omega^2\tau^2}\right)$$

Invariably experimental low-temperature loss peaks are too wide to be explicable in terms of a single relaxation process of the above kind. If we assume a distribution of barrier heights but take $\Delta = 0$ (symmetric case), and D to be constant

$$Q^{-1} = \frac{D^2}{4\varrho c^2 kT}\int_0^\infty \frac{\omega\tau n(V)\,\mathrm{d}V}{1+\omega^2\tau^2} \quad (3)$$

where $n(V)\,\mathrm{d}V$ is the number of two-well systems with barrier height in the range V to $(V + \mathrm{d}V)$. As shown subsequently in Section 4, D is probably not independent of V as assumed, but its variation is slow compared with that of τ and it is satisfactory for present purposes to keep it outside the integral sign. The principal feature of the symmetric case is the inverse proportionality of relaxation strength to absolute temperature. However, if one also assumes a distribution of asymmetries Δ we have

$$Q^{-1} = \frac{2\alpha c}{\omega} = \frac{D^2}{\varrho c^2}\int_0^\infty\int_0^\infty \frac{\mathrm{d}}{\mathrm{d}\Delta}\left(\frac{1}{1+\mathrm{e}^{\Delta/kT}}\right) \times \frac{\omega\tau}{1+\omega^2\tau^2} n(\Delta)n(V)\,\mathrm{d}\Delta\,\mathrm{d}V \quad (4)$$

where $n(\Delta)\,\mathrm{d}\Delta$ is the number of two-well systems with barrier height in the range V to $(V + \mathrm{d}V)$, having asymmetries in the range Δ to $(\Delta + \mathrm{d}\Delta)$. The range of integration for Δ is taken as 0 to ∞ because the averaging of D over all orientations (Section 4) allows for both positive and negative Δ. Assuming a cut-off in the integration at $\Delta = 2kT$ (the contributions to the integral being small for $\Delta \gtrsim 2kT$), and taking $n(\Delta) = n_0$, a constant independent of both Δ and V, one finds [3] that

$$Q^{-1} = \frac{D^2 2n_0}{\varrho c^2}\int_0^\infty \frac{\omega\tau n(V)\,\mathrm{d}V}{1+\omega^2\tau^2} \quad (5)$$

So Q^{-1} now consists of a distribution of SLSLD-type relaxation terms with temperature-independent relaxation strengths. Equation 5 takes the same form as first proposed empirically (but lacking an explicit expression for the constant in front of the integral) by Anderson and Bömmel [4], and used many times subsequently [5, 6].

Apparently if the upper limit in the distribution of asymmetries is $\ll kT$ where presumably T is the highest temperature considered experimentally, Equation 3 will hold, whilst if the upper limit to Δ is $\gtrsim kT$ Equation 5 will hold. In the absence of a satisfactory quantitative theory of the origin of two-well systems it is not obvious which of the two equations, which are effectively at opposite extremes, hold for any given material. It is obvious that in an amorphous material, the local environment to the left of a double well of atomic dimensions will generally differ from the environment to the right, so the presence of asymmetries Δ will be a normal occurrence. However, whereas V is caused by the interaction of nearest-neighbour atoms, Δ represents the effects of next-nearest neighbours (Section 3). Thus it is plausible that on average $\Delta \ll V$, in which case the condition $\Delta \ll kT$ might hold and Equation 3 applies. Clearly it makes sense to try fits of experimental data to both equations. In the present paper, however, we shall consider only Equation 5 which can be written in the form

$$Q^{-1} = \int_0^\infty \frac{C(V)\,\omega\tau\,\mathrm{d}V}{1+\omega^2\tau^2} \quad (6)$$

where

$$n(V) = \left(\frac{\varrho c^2}{D^2 2n_0}\right)C(V) \quad (7)$$

so that the total number of two-well systems (loss centres) per unit volume is

$$n = \int_0^\infty n(V)\,\mathrm{d}V = \left[\frac{\varrho c^2}{D^2 2n_0}\right]\int_0^\infty C(V)\,\mathrm{d}V \quad (8)$$

Gilroy and Phillips [3] have proposed that $n(V)$ takes the form

$$n(V) = \frac{1}{V_\mathrm{p}}\exp\left(\frac{-V}{V_\mathrm{p}}\right) \quad (9)$$

where V_p is the function (which they related to T_g) which determines the shift of the loss peak according to the Arrhenius law

$$\omega\tau_0 \exp\left(\frac{V_\mathrm{p}}{kT}\right) = 1$$

However, one can seek to determine the $n(V)$ function entirely by experiment by fitting Equation 6 to the observed temperature and frequency dependence of Q^{-1}. For this purpose it is more convenient to replace the integral by a sum of the form

$$Q^{-1} = \sum_i \frac{C_i \omega \tau_0 e_i^{V/kT}}{1 + \omega^2 \tau_0^2 e_i^{2V/kT}} \quad (10)$$

where

$$C_i(\delta V)/\delta V = C(V)$$

δV being the interval between the energies in consecutive terms in the sum, i.e. $\delta V = V_i - V_{i-1}$. So

$$\sum_i C_i = \int_0^\infty C(V)\, dV \quad (11)$$

It is of considerable interest to estimate the compositional dependence of n experimentally, both absolutely and expressed as a fraction of the possible number of two-well systems per unit volume of material. However, these estimates will depend on the choice of n_0. Gilroy and Phillips [3] argue that $n(\Delta)$ must be symmetrical about $\Delta = 0$ and that since the width of this symmetrical distribution should be approximately equal to the energy available at the glass transition temperature, for temperatures well below T_g, $n(\Delta)$ will be roughly similar to a constant n_0. Following these authors, if $n(\Delta)$ is assumed equal to n_0 for $\Delta \leqslant V_p$ and $\Delta = 0$ outside this limit we have

$$n_0 = V_p^{-1} \quad (12)$$

and substitution in Equation 8 gives

$$n = \left(\frac{\varrho c^2 V_p}{2D^2}\right) \int_0^\infty C(V)\, dV \quad (13)$$

Although it is hard to justify this *ad hoc* assumption for the form of $n(\Delta)$, it has the advantage that n is expressed in terms of the experimental parameters V_p and $\int C(V)\, dV$ of the acoustic loss process alone. The purpose of choosing a specific form for $n(\Delta)$ is to make possible a discussion of the compositional dependence of two-well systems, and no more. The only quantity in Equation 13 which is not directly measurable from acoustic experiments is D. Values of between 1 to 1.5 eV have been variously proposed in the literature on empirical grounds involving ultrasonic and specific heat data at very low temperatures. An original model of D, relating it to two-well parameters (Section 4), gives a figure of this order but slightly smaller.

3. Microscopic origins of two-well potential systems according to central force theory

3.1. General discussion

We are looking for the possible causes of double well systems with barrier heights of ~ 0.1 eV, which occur copiously in amorphous structures but infrequently in near-perfect crystals. Such low activation energies rule out the translational motion of atoms or groups of atoms arising from the rupture of atomic bonds. Moreover, the size of the attempt frequency $1/\tau_0$ ($\sim 10^{13}$ sec^{-1}) seems to point to the motion of particles of atomic size in potential wells of atomic dimensions.

Consider a three-dimensional network of A–O–A bonds (A = cations, O = anions for example the oxygen atom), where the A–O–A angles are not necessarily 180°. For a perfect crystalline arrangement all A–A separations, and A–O separations (bond lengths) are the same. And for this case central force theory predicts that all anions (or equally the following remarks apply to all cations) move in identical symmetric interatomic wells. Irrespective of the complexity of the vibration which the anion may execute, the wells have a single central minimum corresponding to the equilibrium positions of the anions, and are harmonic for sufficiently small O vibrations, though at larger amplitudes anharmonic effects appear as the wells become flat bottomed. For the amorphous case there will always be a distribution of A–A separations with values both greater and less than the equilibrium (crystalline) value; but with the average size exceeding the latter by a factor $\sim \delta\varrho/3$ where $\delta\varrho$ is the density difference between amorphous and crystalline states. Although this distribution alone is sufficient to define the amorphous state, in some materials there will also be a distribution of A–O bond lengths about the crystalline value. We now examine a number of simple possible transverse and longitudinal motions of the anions in such a material, according to simple classical central force theory.

3.1.1. Longitudinal vibrations

It is generally accepted that to a first-order approximation the mutual potential energy of two atoms in a diatomic molecule takes the form

$$U = \frac{-a}{r} + \frac{b}{r^m} \quad (14)$$

where $6 < m < 12$, and a and b are constants for a given molecular type, which can be obtained from the relationships

$$U_0 = \frac{a}{r_0}\left(1 - \frac{1}{m}\right), \qquad \left(\frac{dU}{dr}\right)_{r=r_0} = 0 \quad (15)$$

where $b = (ar_0^{m-1})/m$. Here U_0 is the bond energy and r_0 is the equilibrium interatomic separation.

Next we consider a linear arrangement of three atoms consisting of an anion in the middle of two cations (or vice versa) separated by a distance R. We assume the potential energy of the system to be given by a superposition of two potentials of the form of Equation 14, i.e.

$$U = \left(\frac{-a}{r} + \frac{b}{r^m}\right) + \left(\frac{-a}{R-r} + \frac{b}{(R-r)^m}\right)$$

so that

$$U = -a\left(\frac{1}{r} + \frac{1}{(2er_0 - r)}\right) + b\left(\frac{1}{r^m} + \frac{1}{(2er_0 - r)^m}\right) \quad (16)$$

where $e = R/2r_0$ is the elongation factor, i.e. the A–A separation divided by the equilibrium separation $2r_0$. The quantity $U/2$ may be regarded as the mutual potential energy of half the O atom plus one of the A

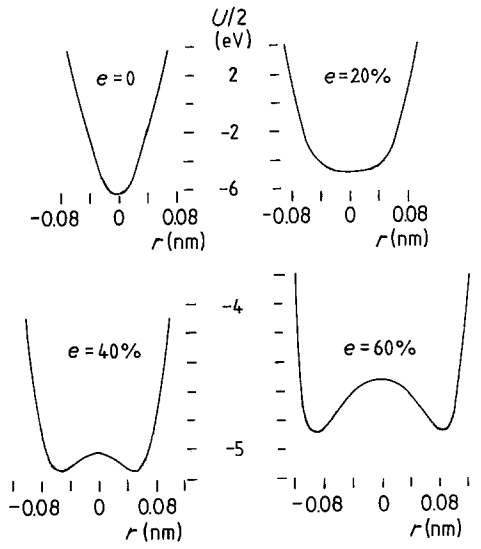

Figure 2 Potential wells for motion of oxygen atoms parallel to P–O–P, for various P–P distances greater than the equilibrium "crystalline" value, in P_2O_5 glasses, calculated from Equation 16, which assumes a 180° P–O–P angle. Central barrier heights are 0.11 and 0.35 eV for elongations of 40% and 60%, respectively.

atoms, and is taken as the potential in which the O atom moves, each A atom being considered infinitely heavy. It should be mentioned that a term allowing for the direct interaction between the A atoms has been ignored. Since it is a function of R only, it does not affect the variation of U with r and is therefore of no interest to us. Of specific interest to us is the P–O–P system for which we take $U_0 = 6.18\,\text{eV}$, $r_0 = 0.156\,\text{nm}$, so that with $m = 9$ we obtain $a = 1.085\,\text{eV nm}$ and $b = 4.229 \times 10^{-8}\,\text{eV nm}^9$.

Fig. 2 illustrates the variation of $U/2$ with position r of the oxygen atom O, for various values of e. It will be observed that the expected single minimum potential occurs for $e < 1$ and also for values of e slightly greater than unity. However, a two-well potential starts to develop for e values above 20%, and for an elongation of 38% a potential barrier occurs of the correct order of magnitude (0.1 eV) to explain the low-temperature loss in amorphous materials.

Pure P_2O_5 glass is about 16% less dense than the high-temperature crystalline form of P_2O_5, corresponding very roughly to an average P–P elongation of 6%, so clearly only a small fraction of the P–O–P

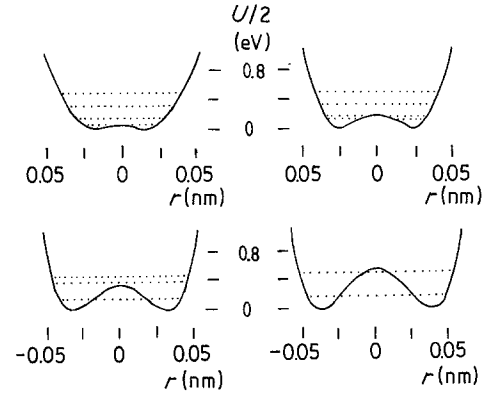

Figure 3 Potential wells for various O–O distances with the four lowest proton states of the system $H_5O_2^+$.

units have the necessary elongation to provide acoustic relaxation, on the above model. However, we shall subsequently find on the analysis of our data that according to Equation 13 only a small number (expressed as a fraction of the number of oxygen atoms per unit volume) of two-well systems are in fact needed to account for the observed losses. Moreover, we suggest that our crude model overestimates the elongations needed to produce two-well potentials. We base this suggestion on the published results of a more rigorous, quantum-mechanical calculation of interatomic two-well potentials for the hydrogen dimer $(H_2O\,OHOH_2)^+$ [7, 8]. These data (Fig. 3) predict barrier heights of ~ 0.1 eV for elongations of only 5% (0.25 nm O–O separation compared with 0.239 nm equilibrium separation). If such a figure holds in the P_2O_5 system, then a substantial fraction of the P–O–P units could be taking part in the loss process.

3.1.2. Transverse vibrations

The potential energy of a linear arrangement of three atoms A–O–A when the O atom is transversely displaced by an amount d (Fig. 4) is, using previous notation,

$$U = \frac{-2a}{(e^2r_0^2 + d^2)^{1/2}} + \frac{2b}{(e^2r_0^2 + d^2)^{m/2}} \qquad (17)$$

Taking the same value of a, b and m as previously, the variation of $U/2$ with d for various values of e, for the P–O–P system, is shown in Fig. 5. For $e > 1$ (elongation) a single minimum only in the potential seen by the vibrating oxygen occurs, but for $e < 1$ potential wells of the order of magnitude required to explain low-temperature acoustic loss (~ 0.1 eV) occur even for a very small contraction of $\sim 6\%$ ($e = 0.94$), suggesting that a large fraction of the O–P–O units in P_2O_5 glass could be contributing to acoustic relaxation by means of transverse two-well vibrations.

3.1.3. Two-well systems with non-180° bond angles

Although the directionality of bonds plays no part in the preceding theory, we did, for simplicity, assume a linear three-atom arrangement equivalent to 180° bonds. However, the theory can readily be extended to the case of A–O–A angles of less than 180°. Hence for the longitudinal vibrational mode shown in Fig. 6 the variation of the mutual potential energy of the A–O–A system with O position d is given by

$$U = \left(\frac{-a}{r_2} + \frac{b}{r_2^m}\right) + \left(\frac{-a}{r_3} + \frac{b}{r_3^m}\right) \qquad (18)$$

where $r_2^2 = d_0^2 + (er_1 - d)^2$; $r_3^2 = d_0^2 + (er_1 + d)^2$; $d_0 = r_0\cos\theta_0$; and $r_1 = r_0\sin\theta_0$.

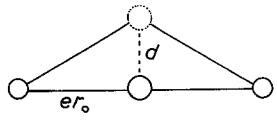

Figure 4 A linear arrangement of three atoms A–O–A when the oxygen atom is transversely displaced by an amount d.

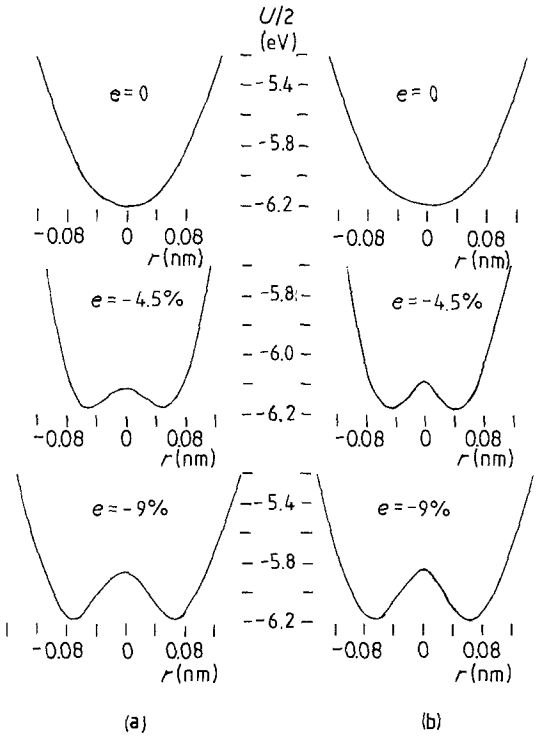

Figure 5 Potential wells for motion of oxygen atoms perpendicular to the P–O–P plane, for P–P spacings less than the equilibrium "crystalline" value, in phosphorus pentoxide glass (a) calculated from Equation 17 which assumes a 180° P–O–P angle and (b) calculated from Equation 19 which assumes P–O–P angle = 140° (the crystalline value). Central barrier heights are (a) 0.066 and (b) 0.087 eV for contractions of 3%; and (a) 0.325 and (b) 0.348 eV for contractions of 6%.

Hence it can be shown that a double well appears when the A–A separation is greater than the equilibrium value $2r_0 \sin\theta_0$, by some critical value of the elongation factor e. We have confirmed this (Fig. 7) for the P–O–P system using the values of a, b and m given previously, and taking $\theta_0 = 70°$ (corresponding to the P–O–P angle in hexagonal crystalline P_2O_5). It will be observed that a two-well potential starts to develop for e values above 25%, and for an elongation of 50%, a potential barrier occurs of the correct order of magnitude (0.1 eV) to explain the low-temperature loss in amorphous materials.

For the case of the transverse vibrational mode illustrated in Fig. 8, the variation of the A–O–A potential energy with O position d is given by

$$U = \frac{-2a}{r} + \frac{2b}{r^m} \qquad (19)$$

where $r^2 = er_1^2 + d_0^2 + d^2$; $r_1 = r_0 \sin\theta_0$; $d_0 = r_0 \cos\theta_0$. Here we expect that for $e > 1$, i.e. an A–A separation greater than the equilibrium value of $2r_0 \sin\theta_0$, only a single minimum occurs in the $U/2$ against d curve, but we suggest that a double-well potential will appear in this curve for some critical value of A–A separation less than $2r_0 \sin\theta_0$ (i.e. $e < 1$). We have confirmed this (Fig. 5b) for the P–O–P system using the values of a, b, m and θ_0 given previously. It will be noted that a barrier height of about 0.1 eV, sufficient to account for the low-temperature acoustic loss in phosphate glasses, occurs for a contraction of only 5% (i.e. $e = 0.95$).

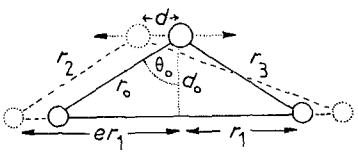

Figure 6 Longitudinal vibration of oxygen atom with non-180° cation–anion–cation bond angle, showing the coordinate system used to calculate two-well barrier heights.

3.2. Comments on the models

(i) It will be noted that the above models predict two-well systems and associated low-temperature acoustic loss peaks in all amorphous materials, since they make no assumptions at all about bond type (directionality). In our opinion this conclusion is supported by the experimental evidence to date. In most of the amorphous materials on which low-temperature acoustic absorption measurements have been made, loss peaks attributable to double-well systems (i.e. standard linear solid, low dispersion, Arrhenius relaxation times, etc.) have indeed been found. In a few cases involving chalcogenides [9], no peaks have been observed. However, this could be because the distribution of barrier heights was so broad as to flatten out the peak, at the operating frequency employed. If we are right in this view the use of higher operating frequencies could reveal the two-well loss peaks, providing ultrasonic detection were still possible at the increased levels of absorption. Alternatively, the peaks might be masked by the presence of other loss mechanisms, for example the thermoelastic loss in metallic glasses.

(ii) Central force theory evidently predicts two-well systems even when the A–O–A bond angle differs substantially from 180° in contradiction with past literature [10, 11] where straight cation–anion bonds were assumed to be required to explain transverse and longitudinal two-well potentials, respectively.

(iii) It will be observed that in the case of transverse anion vibrations, the cation–anion separations in each of the two-well minima may in general differ only slightly ($\lesssim 1\%$) from r_0 even when the cation–cation separation is several per cent less than the crystalline value. The reason for this is that the displacement d of the anion partially cancels the cation–cation contraction. In the case of straight cation–anion–cation bonds, the bond length when the anion is sited in either of the well minima is in fact exactly r_0. Since, classically, the anion will only be observable in the well minima positions, a transverse double well could never show up experimentally in the form of a bond length contraction. This result counters Vukevich's argument [10] that cation–anion bond lengths must be substantially shorter (i.e. several per cent) than the equilibrium (crystalline) value, for transverse two-well systems to occur on central force theory. Much of Vukevich's case against central force theory was based on a presumption that the amorphous state of silica was produced by means of a broad distribution of Si–O–Si bond angles about the cristobalite value of 140°, without any change in Si–O separation. It is true that the Si–O separation corresponding to the peak of

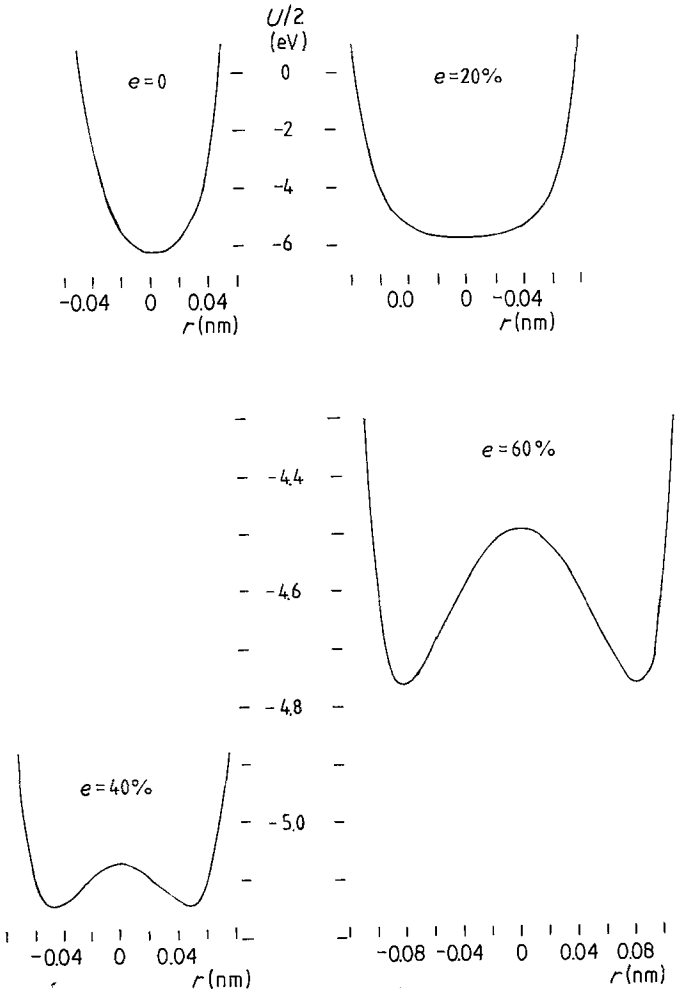

Figure 7 Potential wells for motion of oxygen atoms for various P–P distances greater than the equilibrium "crystalline" value in phosphorus pentoxide glass, calculated from Equation 18 which assumes P–O–P angle = 140° (the crystalline value). Central barrier heights are 0.08 and 0.27 eV for elongations of 40% and 60%, respectively.

the Si–O pair distribution function [12] is almost the same as in cristobalite. However, the half-width of the distribution function is about 6%, consistent with a substantial fraction of Si–O bonds being contracted or elongated by several per cent.

(iv) In the case of longitudinal vibrations, however, in common with Strakna [11], we find that on central force theory two-well systems are possible only for substantial elongations of A–O distances. But subsequent calculations based on Equation 13 (and other arguments given by Vukevich [10] suggest that only a very small fraction ($\sim 1\%$) of two-well systems are in any case required to explain the observed loss. Such a small proportion of stretched bonds, irrespective of the degree of elongation, would never be identifiable as a separate entity on an X-ray radial distribution function (r.d.f.) plot, because of the extent of the overlap of the various pair distribution functions A–O, A–A, (A–2nd O) etc. What we are saying is that the highly elongated bond model must be entertained as a possibility, simply because it cannot be ruled out from experimental r.d.f. data. Strakna's own arguments [11], based on an interpretation of low-temperature specific heat data, required that 10 to 20% of Si–O bonds in vitreous silica be elongated by 20%. Such an occurrence should show up as two separate Si–O peaks (for each of the two-well positions) on r.d.f. plots, and he claimed to find such peaks in X-ray data. We now know that this conclusion was based on inaccurate X-ray data, now superseded.

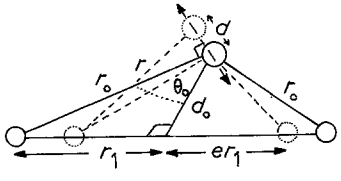

Figure 8 Transverse vibration of oxygen atoms with non-180° bond angle, showing the coordinate system used to calculate two-well barrier heights.

(v) On our central force model, transverse two-well potentials of barrier height near to V_p are generally to be associated with A–O separations only slightly less than r_0, i.e. assuming that the latter corresponds to the peak of the A–1st O pair distribution function $P(r_{A-O})$, the wells are to be associated with separations well up the shoulder on the lower side of the peak. On the other hand, longitudinal two-well potentials are to be associated with A–O separations lying in the tail on the high side of the peak. Thus the most "acoustically active" two-well systems arise from the two shaded regimes of $P(r_{A-O})$ shown schematically in Fig. 9a. Let us write $n(V) = n_T(V) + n_L(V)$, where the subscripts refer to transverse and longitudinal wells, respectively. Now for both kinds of well, barrier height increases with $|r_{A-O} - r_0|$. From the shape of $P(r_{A-O})$ it is clear that $n_L(V)$ will decrease only slowly with increasing $|r_{A-O} - r_0|$ and therefore with increasing V. On the other hand, $n_T(V)$ must decrease very rapidly under the same condition. Combining these two functions (Fig. 9b), the exponential form of the $n(V)$ against V plot proposed by Equation 9 (and found experimentally if Equation 5 is used) can, plausibly, be reproduced. The low "cut-off" value of $n_T(V)$

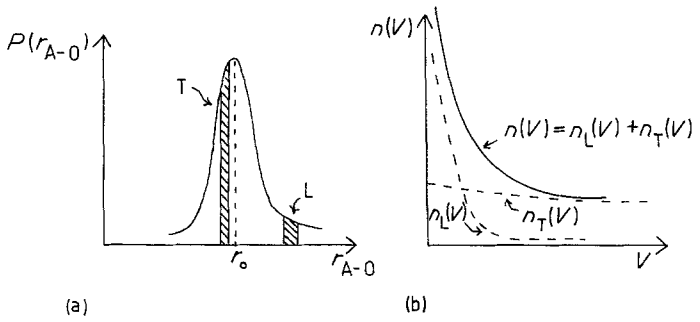

Figure 9 (a) Pair distribution function for A–1st O separations (A = anion, O = cation) in an oxide glass. Shaded regions are to be associated with transverse (T) and longitudinal (L) two-well systems with the "average activation energy" V_p. (b) Form of distribution function for two-well systems proposed from (a).

at $V = 0$ stems from the fact that V remains at zero until $|R_{A-O} - r_0|$ has increased to a substantial size. The value of $n_L(V)$ at $V = 0$ is much higher, since transverse double wells arise as soon as $|R_{A-O} - r_0|$ exceeds zero.

(vi) For any one two-well system A–O–A, further O atoms to the left and right of the A atoms will generally be situated at slightly different distances from the latter. Thus on our simple central force model a distribution of asymmetries Δ will appear as a second-order (next-nearest neighbour) effect.

4. Theoretical expression for deformation potential *D*

Attempts to derive a fundamental formula for D have not yet been reported in the literature. The value of about 1 eV widely quoted, assumed independent of activation energy, and used in our previous calculations, has been obtained experimentally from very low temperature (< 4 K) specific heat and ultrasonic data on some glasses. The following simple original theory predicts a deformation potential which is an increasing function of two-well barrier height V. If experimental average activation energies are substituted into our formula, potential values in rather close agreement with the empirical values are obtained.

The number of cation–anion–cation units (A–O–A units) in 1 m^3 of glass is $n_b N_a/M$, where N_a is Avogadro's number (per kilomole), M is the mass of one kilomole and n_b is the number of A–O–A units per formula unit.

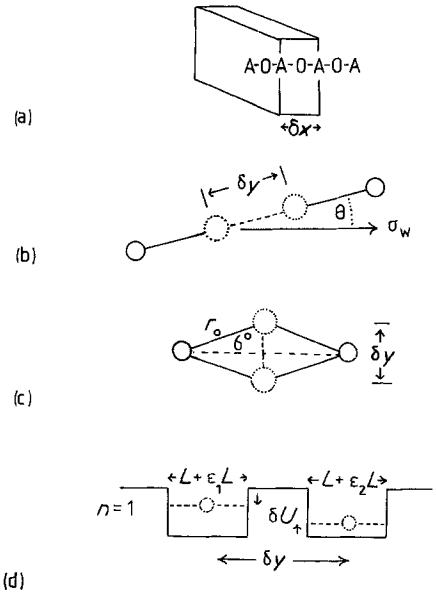

Figure 10 Variables considered in a treatment of the deformation potential.

The number of these units intersecting any cross-section of unit area (m^2) is $n_b N_a \varrho \delta x/M$, where δx is the A–A separation (Fig. 10a).

Now assuming a continuum, the force field per unit area due to the applied stress field is $\sigma = q\varepsilon$, where ε is the strain and the elastic modulus $q = K + (4/3)G$ for a longitudinal wave, K and G being the bulk and steel moduli, respectively. So assuming a continuum, the force field experienced by one vibrating oxygen atom is

$$\sigma_w = \frac{q\varepsilon}{n_b N_a \varrho \delta x/M} \tag{20}$$

Suppose for a given A–O–A two-well system the minima are separated by a distance δy, and the line joining these minima is inclined to the force field at an angle θ, then the work done by the acoustic stress field on an oxygen atom when the latter is thermally activated from one well to another, is (Fig. 10b)

$$\sigma_w \cos\theta \delta y = \frac{q\varepsilon \cos\theta \delta y}{n_b N_a \varrho \delta x/M} \tag{21}$$

Compare now with the Jäckle *et al.* [2] definition of deformation potential, i.e. that the shift in the minima of the two-wells due to the acoustic interaction is

$$\delta U = D\varepsilon \tag{22}$$

Comparing Equations 21 and 22, we find that for the two-well system under discussion

$$D = q\left(\frac{M}{n_b N_a \varrho}\right)\frac{\delta y}{\delta x}\cos\theta \tag{23}$$

An average value of deformation potential appropriate to a macroscopic glass sample is obtained by averaging over all possible values of $|\theta|$. If we assume equal probabilities for the A–O–A lines to occur in any orientation relative to the field direction (as to be expected for an amorphous i.e. isotropic material), the average value of $|\cos\theta|$ is 1/2. So

$$\bar{D} = \frac{q}{2}\frac{M}{n_b N_a \varrho}\frac{\delta y}{\delta x} \tag{24}$$

where it is emphasized again that δx = normal cation–cation separation and δy = separation of minima in the two-well potentials.

Since the barrier height V increases with δy (Figs 2, 5 and 7) the deformation potential will increase with activation energy.

To find the order of magnitude of D given by our theory we consider a few specific examples below. Values of q and ϱ are taken from Table I in all cases. In addition, for SiO_2 and P_2O_5 glass n_b is assumed to

TABLE I Low-temperature properties of molybdenum–phosphate glasses*

Glass reference no.	Density ($g\,cm^{-3}$) ± 0.002	Longitudinal wave velocity, c (300 K) ($m\,sec^{-1}$)	MoO_3 (mol %) $\pm 1\%$	Peak temperature (K) ± 1	Peak loss ($dB\,sec^{-1}$) ± 0.05	Frequency, v (MHz)	Attempt frequency, τ_0^{-1} ($\times 10^{13}\,sec^{-1}$) ± 0.02	Activation energy determined from peak shift, V_p (eV) ± 0.005	$\int C(V)\,dV$ ($\times 10^{-3}$) ± 0.5	Number of loss centres, n ($\times 10^{21}\,cm^{-3}$)	Number of loss centres per oxygen atom, N(%)
A/4	2.753	4146	29.2	128	6.63	44.0	0.30	0.123	84.3	1.53	3.02
A/6	2.840	4206	37.5	107	5.92	44.0	0.87	0.111	79.8	1.39	2.76
A/8	2.936	4280	44.2	104	5.75	44.0	0.78	0.107	70.4	1.26	2.52
A/10	2.969	4310	47.4	94	4.86	44.0	1.29	0.102	65.5	1.15	2.32
A/19	3.090	4288	55.0	90	4.81	44.0	2.06	0.102	59.5	1.08	2.18
A/25	3.207	3996	61.6	83	5.63	44.4	1.35	0.091	70.5	1.03	2.05
A/37	3.352	4032	69.5	75	6.14	44.0	0.60	0.079	84.6	1.14	2.27
A/44	3.592	4063	80.8	74	6.48	45.0	0.24	0.070	83.2	1.08	2.13
SiO_2	2.200							0.05	33	0.41	0.9

*The glass reference number allows cross-referencing to glass data in other publications. The quoted errors do not apply to fused silica, data for which have been taken from Anderson and Bömmel [4].

be 2 and 3, respectively, neglecting non-bridging bonds in the case of P_2O_5.

4.1. SiO_2 glass

On the cation–cation elongation model, δy for a two-well potential of barrier height equal to the average activation energy (1200 kcal mol^{-1} = 5021 kJ mol^{-1}) is 0.042 nm (Table I of [11]). So taking δx = 0.32 nm for the normal Si–Si separation, we find D = 0.73 eV. On the other hand, if the cation–cation contraction model is taken, the value of δy (Fig. 10c) corresponding to a bond angle shift of $\pm 6°$ from normal (which Anderson and Bömmel [4] claimed produced a barrier corresponding to the average activation energy of the observed acoustic loss), is 0.0334 nm. From this we find D = 0.6 eV.

4.2. P_2O_5 glass

As data from the literature are unavailable, we have estimated values of δy (corresponding to well barrier heights equal to the average activation of the observed acoustic loss) from our own two-well potential models. On the elongation model, extrapolating from Fig. 2, we find that δy, corresponding to an average activation energy of about 0.15 eV, is about 0.06 nm. Taking x = 0.312 nm, this yields D = 0.77 eV. On the other hand, extrapolating from Fig. 5a, the value of δy corresponding to an average activation energy of 0.15 eV on the contraction model, is about 0.05 nm. This result gives D = 0.65 eV.

As V and $\Delta \to 0$ the acoustic loss for n two-well systems approaches the value $\alpha = nD^2\omega^2\tau_0/8\varrho c^3 kT$ (with $\omega\tau_0 \ll 1$). The single well corresponding to this limit will generally be anharmonic, being flatter bottomed than a harmonic well in the case of elongated cation–cation spacings, and with steeper walls than a harmonic well in the case of contracted cation–cation spacing. So it is tempting to identify the above attenuation limit with the attenuation due to phonon–phonon interaction in the limit $\omega\tau \ll 1$, i.e. $\alpha = c_V T\gamma^2\tau_{th}/2\varrho c^3$, where c_V is the heat capacity per unit volume, γ is some kind of average Gruneisen constant for the phonon modes in the material, and τ_{th} is the mean lifetime of thermal phonons. In this case

$$D \sim \gamma T\left(\frac{4c_v k}{n}\right)^{1/2} \quad \text{for } V \to 0 \qquad (25)$$

The value of D calculated by substitution of appropriate constants is extremely small compared with 1 eV. Evidently the coupling in the two-well acoustic loss mechanism ($D \sim$ 1 eV) is extremely strong compared with the phonon–phonon interaction.

Compressional waves produce adiabatic deformation of the quantum states in each potential well, and a corresponding contribution to the deformation potential might be expected. However the effect is very small, as can be shown from the following simple analysis of a one-dimensional rectangular-shaped double well (Fig. 10d). The permitted kinetic energy levels for each well in the absence of the wave are $KE = n^2h^2/8mL^2$, where n is a quantum number 1, 2, 3..., h is Planck's constant, m is the particle mass, and the remaining notation is as in the figure. So when a wave is present, corresponding levels in each well, i.e. the kinetic energies for each quantum level (n value) in the two wells shift by an amount

$$\delta U = 2(KE)(\varepsilon_1 - \varepsilon_2) \approx \mathrm{j}(2\,KE)\varepsilon k\,\delta x \qquad (26)$$

where ε_1 and ε_2 are the strains in each well region, and in the second equation on the right hand side, $\varepsilon \sim \varepsilon_1 \sim \varepsilon_2$, k is the wave vector for a sinusoidal wave, δx is the well separation, and the imaginary number $\mathrm{j} = (-1)^{1/2}$ denotes that δU is in phase quadrature with ε. Comparing with the Jäckle *et al.* [2] definition of deformation potential,

$$D = \mathrm{j}(2\,KE)k\,\delta x, \qquad (27)$$

and its magnitude is easily shown to be extremely small compared with 1 eV, at megacycle frequencies.

5. Experimental details: acoustic loss and velocity (longitudinal wave velocity) measurements at low temperatures in Mo–P–O glasses

Acoustic wave loss and velocity for longitudinal waves in the range 4.2 to 300 K in Mo–P–O glasses were measured simultaneously using standard pulse-echo techniques. However, only the loss measurements are to be discussed in this paper. Arenberg ultrasonic instrumentation (PG 650-C power oscillator, PA 620 5 to 60 MHz preamplifier, VR-720 50 to 230 MHz amplifier, WA-600-E 5 to 60 MHz video amplifier, and ATT-693 1 to 122 dB attenuator), was employed (Arenberg Sage Inc., Boston, USA).

Temperature control was effected with purpose-built equipment supplied by Oxford Instruments Ltd. (Oxford, UK). The cryostat was a low-consumption continuous flow type (CF 500), with the standard 20 mm cylindrical low-temperature chamber enlarged to a diameter of 25 mm.

All operations on the cryostat were performed from a mobile pumping trolley containing pumping apparatus, flow controller, and temperature controller (DTC2). It was not economical in terms of either time or liquid helium consumption to perform measurements on the large number of Mo–P–O glasses that had been prepared to map out the unusual compositional dependence of physical properties at room temperature [13, 14]. Eight glasses were therefore selected which (i) spanned the entire vitreous compositional range, and (ii) defined adequately the regions in which the other physical properties had been found to change rapidly with composition. The glass discs of diameter 1.6 cm and 5 mm thickness had end-faces polished optically flat and parallel to 1 to 2 seconds of arc, using a Multipol 11 polishing machine and a precision polishing jig, adjusted via an autocollimator (Metals Research Ltd., Cambridge, UK). The specimens were coated with vacuum-evaporated aluminium to provide an earth electrode, and allow the use of uncoated X-cut quartz transducers. A single 15 MHz transducer was employed as both a sender and receiver of pulses and provided all the operating frequencies employed by harmonic excitation. Precise operating frequencies were adjusted to achieve the best exponential decay pattern rather than maximum

echo height. Nonaq stopcock grease was found to provide a satisfactory bond down to the lowest temperature employed. Excess grease exuded during the adjustment of the transducer–bond specimen combination for the best echo pattern had to be removed carefully with acetone, otherwise bonds were found to break at about 130 K.

The average value of the dB differences between several pairs of echoes was used in obtaining the absorption value either in dB cm^{-1} or dB μsec^{-1} or in terms of internal friction Q^{-1}. Measurements were performed simultaneously at every 5 K (± 0.1 K) temperature rise, starting from the lowest temperature achieved by the cryostat. Such an experimental run took about 6 h after 0.5 h for cool-down, and five runs were usually obtainable from a 17-litre Dewar flask of helium. Investigation of each glass sample (four runs at different operating frequencies plus one velocity measurement run) thus consumed one Dewar of helium. The temperature of the specimen was monitored by two pre-calibrated gold–chromel copper–constantan thermocouples which were attached to a specimen. In all our measurements the error in attenuation was ± 0.5 dB per transit and the error in temperature was $\pm 0.2°$ C.

6. Analysis of results: peak shift and distributions of relaxation times

Typical results showing the temperature dependence of the absorption at about 44 MHz are illustrated by data points given in Figs 11a and b for all Mo–P–O glasses of different compositions (see Table I).

Figs 12a to h illustrate by data points the comparatively small shift in peak temperature with frequency (compared for example with borate glasses), which is characteristic of these glasses. For example, Specimen A/2 (29.2 mol % MoO_3) shows a shift in peak temperature from 116 K at 14 MHz to 139 K at 106 MHz. The attenuation, especially at the peak temperature, increases rapidly with the frequency, and thus limited our measurements up to between 105 and 135 MHz.

Plots of log ω against inverse peak temperature T_p^{-1} (Figs 14a and b) yield straight lines, showing that for a given glass the peaks fit an equation of the form $\omega\tau_0 \exp(V_p/kT) = 1$, where τ_0 and V_p are constants determined from the intercept and the slope of the lines, respectively. The values of τ_0 thus obtained (Table I) are of the same order of magnitude (i.e. 10^{13} Hz^{-1}) as have been found for other glasses; whereas V_p, which decreases with MoO_3 content and ranges from 0.0698 to 0.123 eV, is much higher than the value for vitreous silica (0.05 eV) [4]. Fig. 13, together with the slow variation of velocity with temperature (to be discussed elsewhere), suggests that an SLSLD type of loss process is operative, as in other glasses. But the width of the peaks indicate that a single relation time with $\tau = \tau_0 \exp(V_p/kT)$ is an inadequate description. Rather, V_p is some kind of average over a broad distribution of activation energies, and we propose to fit Q^{-1} to a distribution of the form of Equation 10, with τ_0 assumed constant. The value of the relaxation strength C_i for each activation energy V_i was then calculated for all eight glasses (Table I). In order to achieve this, 26 activation energies ($V + \delta V$) were selected, ranging from about 0.01 to 0.26 eV (differing slightly for each specimen; see Figs 14a and b), in steps of equal intervals of δV (e.g. 0.0104 eV for Sample A/2, 0.011 eV for Sample A/5 and so on), so that Equation 10 represented a close approximation to a continuum distribution. Further, 26 different temperatures were selected in 10 K intervals starting from 10 K, and 26 different corresponding values of Q^{-1} were read off

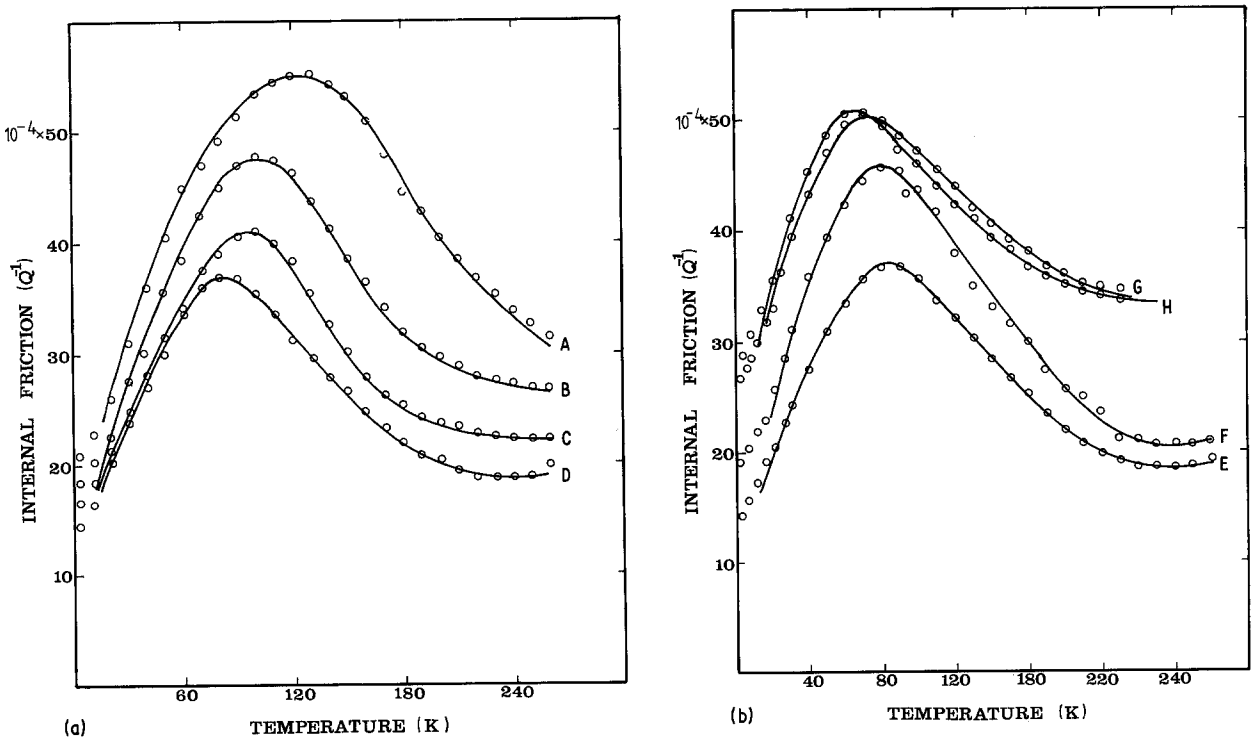

Figure 11 (a, b) Temperature dependence of ultrasonic wave loss in terms of internal friction at 44 MHz. Circles represent the experimental data and solid lines show a theoretical fit to Equation 10 (the latter being an approximation to Equation 5), as explained in the text. MoO_3 content (mol %) as follows: (A) 29.2, (B) 37.5, (C) 44.2, (D) 47.4, (E) 55.0, (F) 61.6, (G) 69.5, (H) 80.8.

the experimental 44 MHz loss curves. Substitution of all these Q^{-1}, V and T values into Equation 10, and solving the resulting 26 simultaneous equations with 26 undetermined constants C_1, C_2, ... C_{26} by computer programming, the spectrum of relaxation strengths for each glass can be obtained.

Generally an exact solution thus obtained will contain some negative values of C_i, especially at high values of $(V + \delta V)$, which can have no physical meaning. When this occurred the chosen values of V and δV were adjusted slightly until a solution involving only all positive values of C_i was obtained. A smooth curve was then drawn through these values. To ensure that these values of C_i will give back the correct values of α (i.e. reproduce the experimental $Q^{-1}-T$ curve), using the same Equation 10, we had to further adjust the shape of the smooth C_i against V curve. After achieving this, the final graphs of C_i against V are presented in Figs 14a and b for each glass.

In addition, the final set of relaxation strengths obtained at about 44 MHz for each glass gives a close fit (solid lines) to the experimental absorption data (full circles) at all other frequencies employed. The upper and lower cut-off energies 0.01 and 0.26 eV used in the above analysis have no physical significance, but merely relate to the problems of computing.

Although the overall form of the experimental $C(V)$

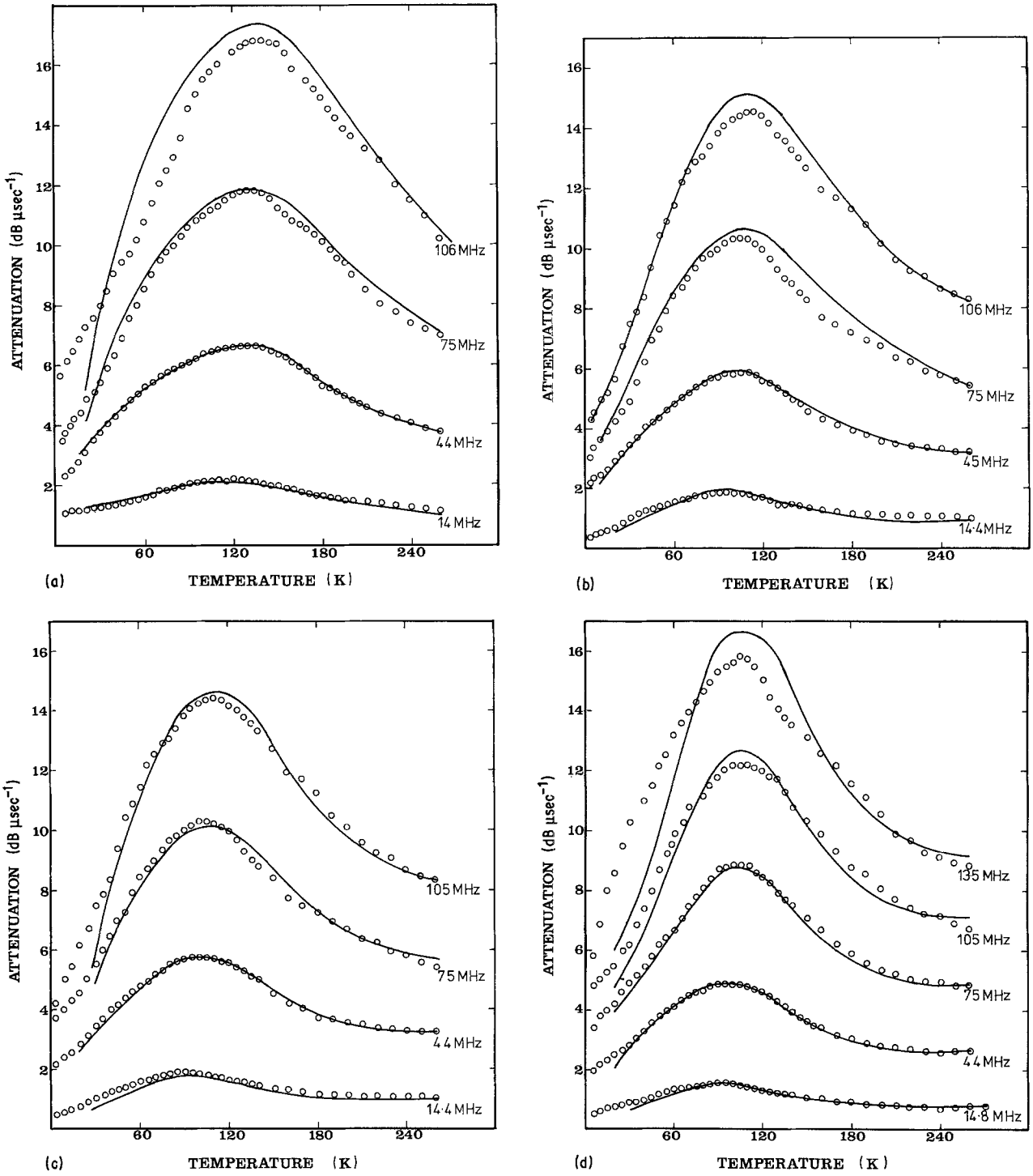

Figure 12 Temperature dependence of the attenuation of longitudinal sound waves in Mo–P–O glasses. Circles represent the experimental data and solid lines represent a theoretical fit of the data to Equation 10 (as an approximation to Equation 5) as explained in the text. MoO_3 content (mol %) as follows: (a) 29.2, (b) 37.5, (c) 44.2, (d) 47.4, (e) 55.0, (f) 61.6, (g) 69.5, (h) 80.8.

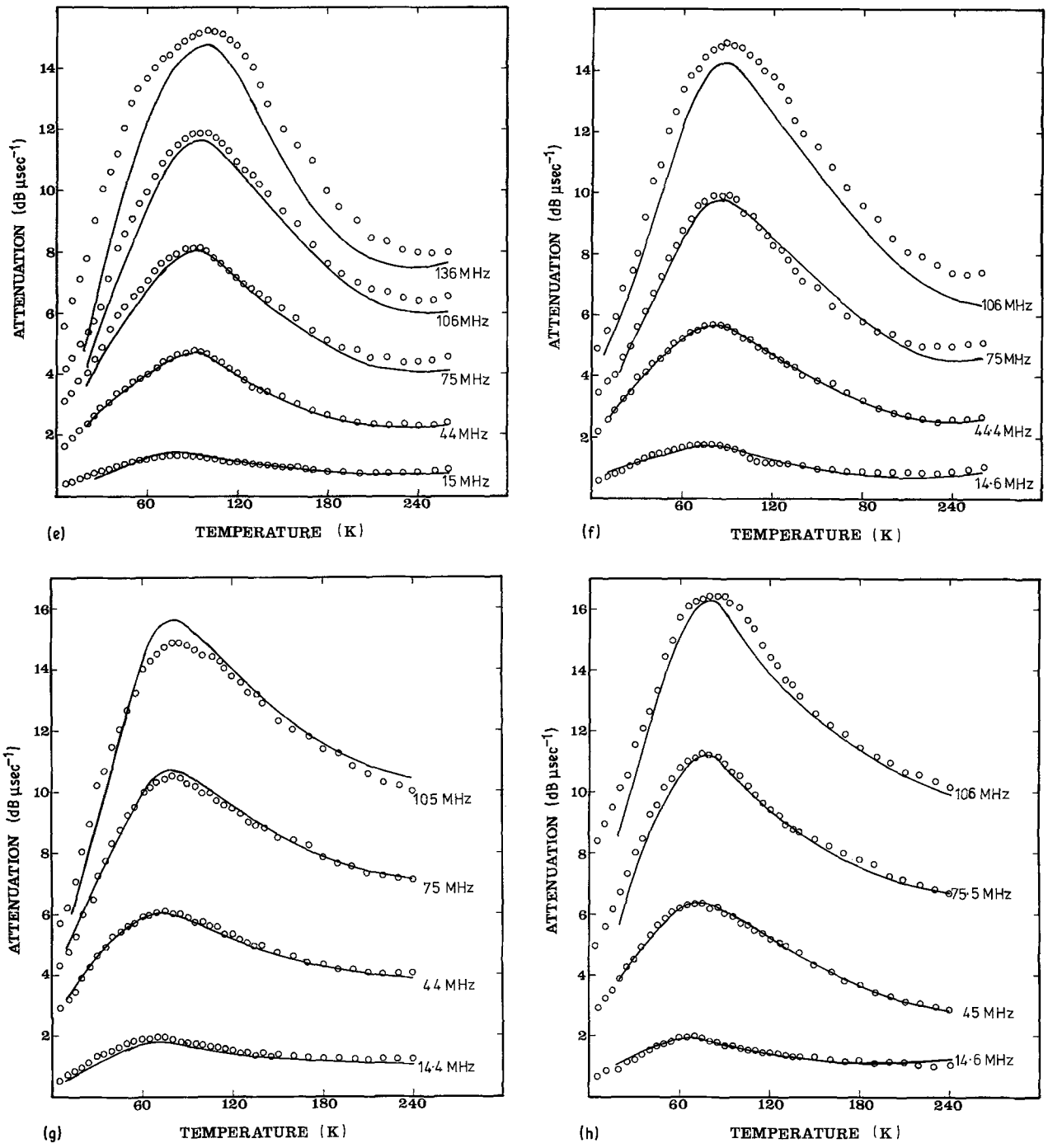

Figure 12 Continued.

against V functions follow the general trend suggested by Equation 9, i.e. a rapid decrease of $C(V)$ with V of roughly exponential form, there are important differences in detail. Whereas in these Mo–P–O glasses V_p varies linearly with composition, $\int C(V)\,dV$ displays a sharp minimum at 50 mol % MoO_3, with some evidence of a second turning point (a small maximum) in compositional gradient at 66 mol % (Fig. 15). Clearly this conflicts with the relation of Gilroy Phillips [9] (Equation 9) which proposes a systematic and monotonic relationship between the two quantities. The value of performing composition-dependence experiments should now be clear.

To estimate the total number of two-well potentials contributing to the acoustic loss (loss centres) per unit volume from Equation 13, we use the glass ϱ, c, V_p and $\int C(V)\,dV$ data given in Table I. For D we adopt a nominal value of 1 eV. Expressed as a fraction of the number of oxygen atoms per unit volume it will be noted that the number of loss centres in these phosphate glasses is two to three times higher than the number in vitreous silica. The compositional dependence of n (Fig. 16) shows evidence of a pronounced minimum followed by a weaker maximum at high MoO_3 content, and seems to be systematically related to the compositional dependence of the elastic moduli [14], i.e. n decreases as the moduli increase. This is one factor which affects our interpretation of data in the following sections.

7. Comparison of the low-temperature ultrasonic loss and relaxation spectra in molybdenum–phosphate and SiO_2 glass

In Fig. 17 the low temperature internal friction peak in our glasses is compared with similar observations on

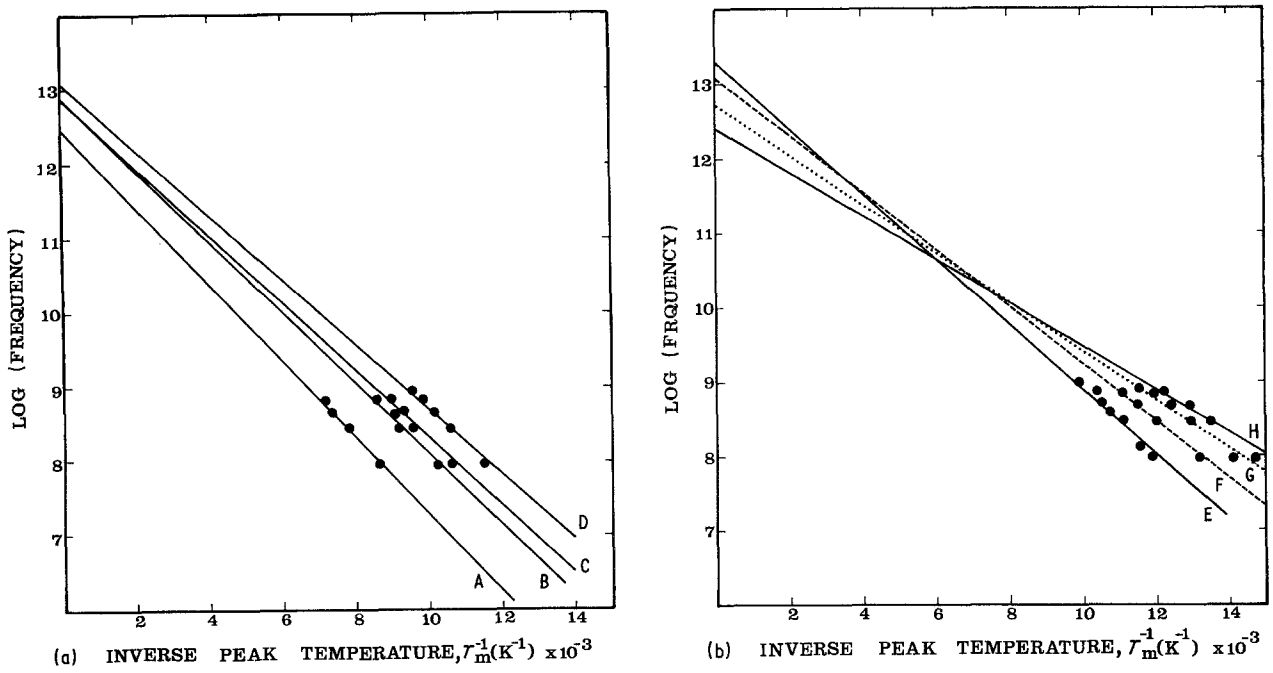

Figure 13 (a, b) Experimentally observed relation between the logarithm of the measurement frequency ($\omega = 2\pi\nu$) and the inverse peak temperature for the attenuation of compressional waves in Mo–P–O glasses. MoO_3 content (mol %) as follows: (A) 29.2, (B) 37.5, (C) 44.2, (D) 47.4, (E) 55.0, (F) 61.6, (G) 69.5, (H) 80.8.

a number of other inorganic oxide glasses [1, 15]. However it is of special interest to compare our phosphate glasses with vitreous silica, whose low-temperature properties have been reported in the literature more thoroughly than for any other glass. The ratio of $n(MoO_3–P_2O_5$ glass$) : n(SiO_2$ glass) is typically about 1.5 to 2 and is roughly the same as the ratio of the corresponding peak temperature losses. However, it is of greater interest to explain the much more pronounced differences in the loss behaviour of SiO_2 and these Mo–P–O glasses that arise when the temperature dependence is considered. For example (Fig. 17) in the temperature range 4 to 30 K the Q^{-1} in our glasses with about 50 mol % MoO_3 is almost the same as that in SiO_2 glass. But with increasing temperature Q^{-1}(Mo–P–O glass)/Q^{-1}(SiO_2 glass) increases

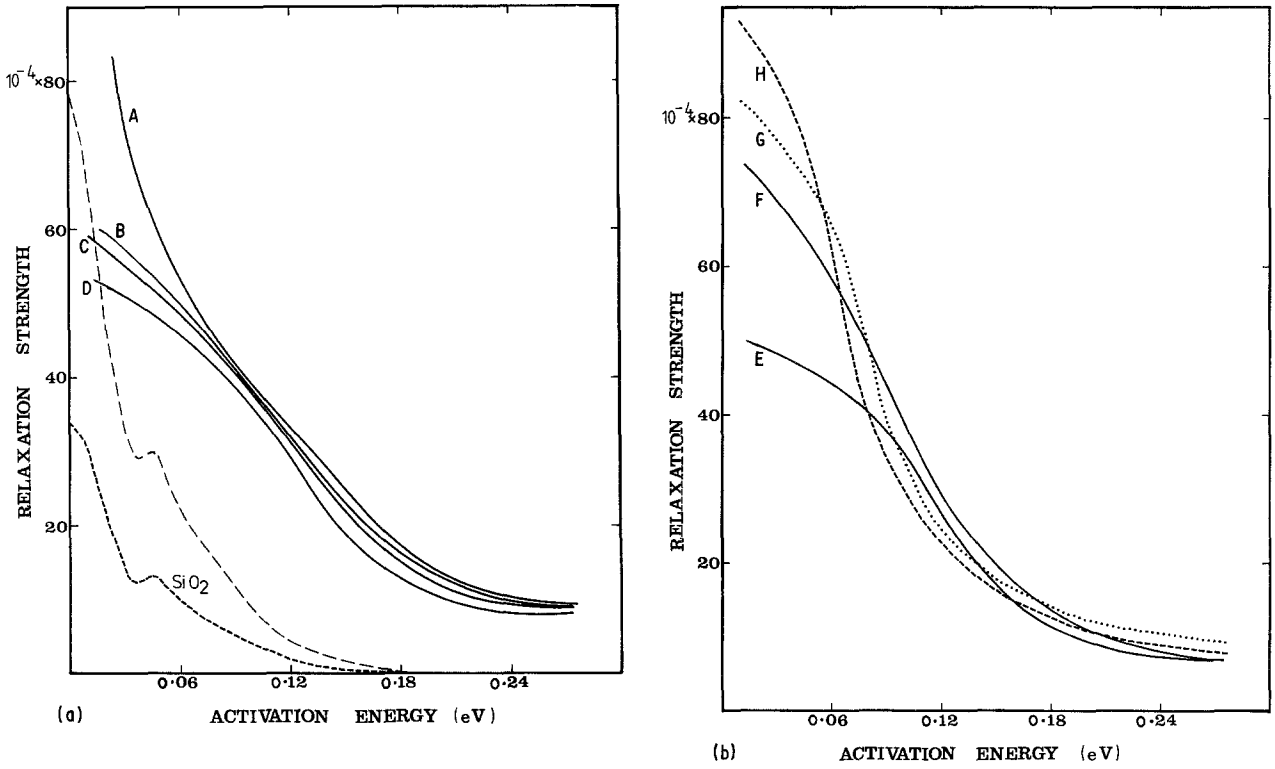

Figure 14 (a, b) Relaxation spectrum $C_i(\delta V)$ against V obtained from a computer fit of the equation $Q^{-1} = \Sigma_i C_i \omega\tau_0 e^{V_i/kT}/(1 + \omega^2\tau_0^2 e^{2V_i/kT})$ to the low-temperature ultrasonic wave loss in Mo–P–O glasses. MoO_3 content (mol %) as follows: (A) 29.2, (B) 37.5, (C) 44.2, (D) 47.4, (E) 55.0, (F) 61.6, (G) 69.5, (H) 80.8. Summation intervals $\delta V = V_{i+1} - V_i$ of 0.0104 eV were used for Glasses A, B, G and H, whilst intervals of 0.011 eV were used for Glasses C, D, E and F. SiO_2 data included for comparison have been taken from Anderson and Bömmel [4]. Here δV = 0.01 eV and 0.004 eV for the upper and lower curves, respectively.

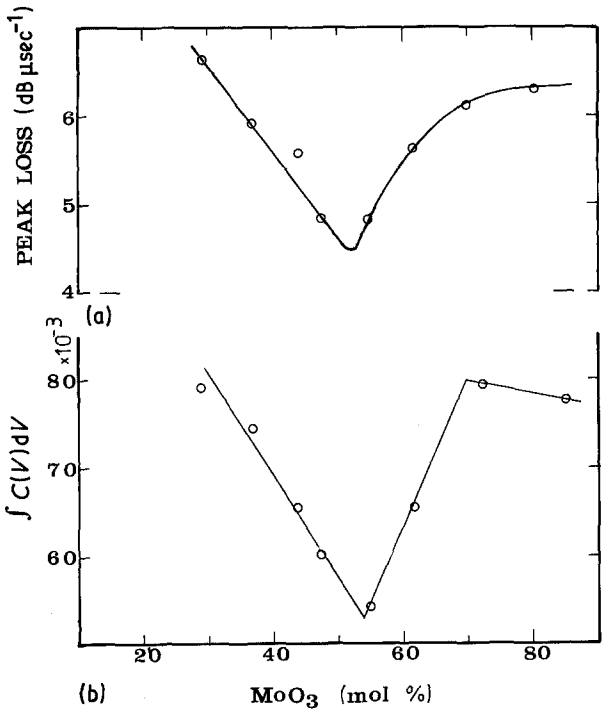

Figure 15 Compositional dependence of the low-temperature acoustic loss in Mo–P–O glasses, expressed in terms of (a) the peak loss, and (b) the quantity $C(V)\,dV$ as defined by fitting the experimental loss to the equation $Q^{-1} = \int C(V)\,dV\omega\tau_0 e^{V/kT}/(1 + \omega^2\tau_0^2 e^{2V/kT})$. With respect to the numerical integration used in our computer fit $C(V) = C_i(\delta V)/\delta V$.

rapidly, so that at 150 K the loss in the phosphate glass is more than 20 times larger than the loss in vitreous silica. This behaviour can be nicely explained in terms of the relative shape of the relaxation spectra ($C_i(\delta V)$ against V curves) of these glasses displayed in Figs 14a and b. The spectra are roughly comparable in height and shape at sufficiently low activation energies, and

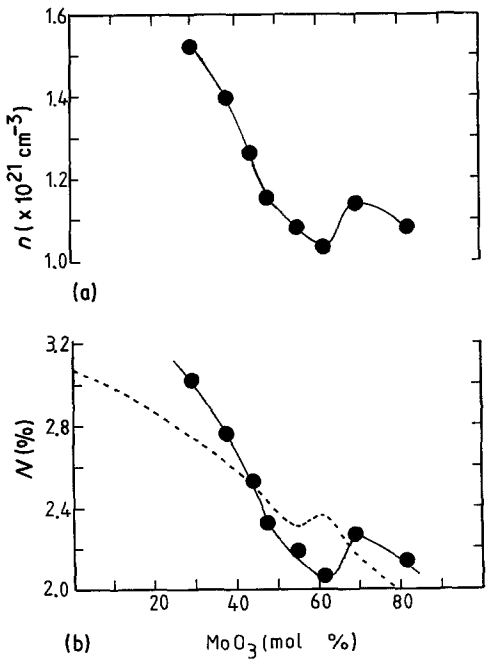

Figure 16 Compositional dependence of (a) the number of loss centres n (interatomic two-well potentials) operative in the low-temperature acoustic loss, and (b) number of loss centres N expressed as a function of number of oxygen atoms per cm^3 (in molybdenum–phosphate glasses). The solid line is drawn through experimental data points and the dotted line is the theoretical curve predicted by Equation 37.

it is the much longer and thicker tail on the spectral distribution of the phosphate glasses that is responsible for their (relatively) very high loss at higher temperatures, as will be shown in the detailed arguments below.

To assist the interpretation of these spectra we first consider Fig. 18, which illustrates the overall attenuation plotted as a function of T at constant ω as a superposition of relaxation terms having a spread of activation energies V_1, $V_2 \ldots V_i$, where for simplicity the "relaxation strengths" C_i have been assumed all equal to unity.

It is now clear how this superposition of peaks combined with a distribution function $C_i(\delta V)$ against V, which increases with decreasing V, yields an overall curve which has a peak which is steeper on the low T side than on the high T side. However, at the moment we are interested in the shape and position of the individual relaxation terms. It is easily shown that the loss peak produced by a loss centre with activation energy of V, occurring at a temperature $T_p = -(V/k\ln\omega\tau_0)$, has a width

$$\Delta T = -\frac{V}{k}\left[\frac{1}{\ln(\omega\tau_0/0.414)} - \frac{1}{\ln(\omega\tau_0/2.414)}\right] \tag{28}$$

at the "half-power points", i.e. the points at which the loss has fallen to $1/2^{1/2}$ of the peak value. Correspondingly, at a temperature T only those loss centres having activation energies in the range $\Delta V = k\Delta T$, centred on $V_p = -kT\ln\omega\tau_0$, may be considered to be "highly activated". For an even distribution of activation energies (i.e. flat C_i against V spectrum) most of the overall loss at a temperature T would then arise from loss centres having activation energies in the range ΔV. However, the shape of the C_i–V spectra observed in our glasses (and others) throws an increased weighting on activation energies of low value so that the loss due to "weakly activated" loss centres is significant. Even so it will remain true that a significant fraction of the overall loss at a temperature T will arise from the energy range ΔV centred on $V_p = -kT\ln\omega\tau_0$ and the amount of this loss will be

$$Q^{-1}_{\Delta V} \sim \frac{1}{2}\frac{C_i(\delta V)\Delta V}{\delta V} \tag{29}$$

(where the factor 1/2 arises from the peak value of each relaxational term), i.e. we are proposing that the loss at a given temperature can be roughly correlated with the value of C_i at a given point of the C_i against V spectrum.

For example, at low temperatures like 10 K only loss centres with $V \approx 0.01$ eV are "activated". Inspecting the relaxation spectra (Figs 14a and b), we observe that for this energy the values of $C_i(\delta V)$ for the Mo–P–O glasses and SiO_2 glass are of the same order. Correspondingly, by Equation 29 the losses are of the same order, in agreement with practice (Fig. 17).

On the other hand at a high temperature like about 200 K only loss centres with $V \sim 0.2$ eV are activated. And inspecting the relaxation spectra in this range we

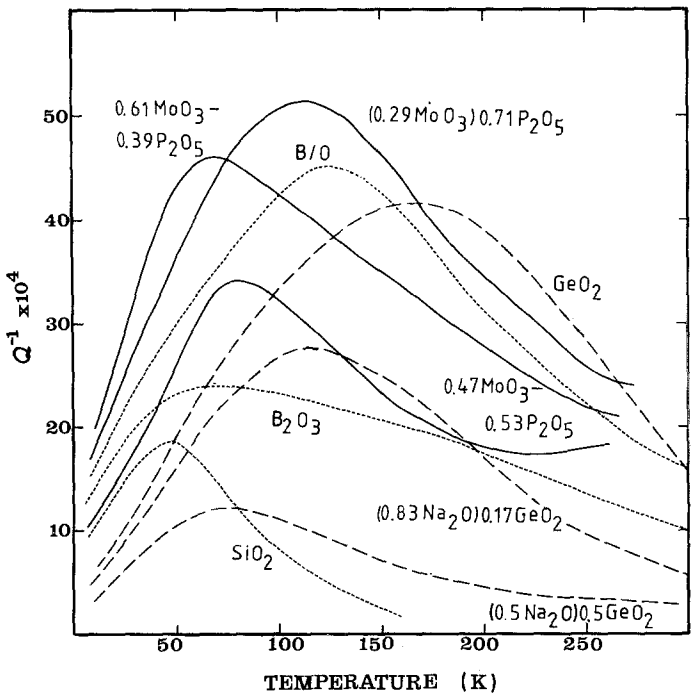

Figure 17 Comparison between the internal friction peak observed in a number of inorganic oxide glasses. Dashed lines, data are taken from results of other workers: GeO_2 and Na_2O-GeO_2 (Krause and Kurkjian [15]), SiO_2 (Anderson and Bömmel [4]), B_2O_3 and $Na_2O-B_2O_3-SiO_2$ (B/O) (Maynell *et al.* [1]). Solid lines are from Mo–P–O glasses of this study. Figures denote mole fractions.

find that $C_i(\delta V)$ for phosphate glasses is about 20 times the value for vitreous SiO_2, in close correspondence with the observed loss levels.

8. Interpretation of the compositional dependence of low-temperature acoustic loss in glasses

Essentially we shall use the central force model of the origin of acoustically active two-well systems, described in Section 3. We regard Mo–P–O glasses as three-dimensional networks [13, 14] in which P–O–P, P–O–Mo and Mo–O–Mo bond angles will have a spread of values around the fixed values obtaining in crystalline molybdenum phosphates. Correspondingly, there will be a spread of cation–cation (P–P, Mo–P and Mo–Mo) spacings, these spacings being smaller than the equilibrium (crystalline) values for bond angles more acute than normal, and larger for bond angles straighter than normal. As before it will be acceptable to talk just about the motion of oxygen atoms – a reasonable viewpoint given the relative mass of the molybdenum and phosphorus atoms. On central force theory a distribution of two-well systems for transversely vibrating oxygen atoms will arise from the spread of cation–cation spacings. And if there is also a spread of bond lengths, a distribution of longitudinal two-well systems will also occur. Our interpretation must take place without radial distribution function data (X-ray or neutron diffraction), since these are unavailable for phosphate glasses.

8.1. Effect of number of oxygen atoms per unit volume (oxygen density)

If the above simplification of interatomic two-well systems in terms of oxygen atoms vibrating between static heavier atoms is correct, one would expect that the total number of acoustically active two-well systems (total number of loss centres) will be proportional to oxygen density.

8.2. Effect of atomic ring size

In the subsequent interpretation of the dependence of two-well systems on glass composition, it will be convenient to envisage the structure of oxide glass as a three-dimensional network of atomic rings, where a ring is the shortest closed circuit of atomic bonds [16].

The variability of the P–O–P, P–O–Mo and Mo–O–Mo bond angles means that there will be a spread of atomic ring sizes in the glasses. And since the production of the amorphous state from a given crystalline state always leads to a density decrease, we know that the average atomic ring size in a given Mo–P–O glass will be larger than the ring sizes occurring in the nearest equivalent crystalline molybdenum–phosphate, although there will be some rings smaller than the crystalline one.

There are clearly more opportunities to achieve a distribution of cation–anion–cation angles in large rings than in small ones. For example a sequence of 180° bonds will produce a very large ring, whilst relatively few 180° bonds will be possible in a very

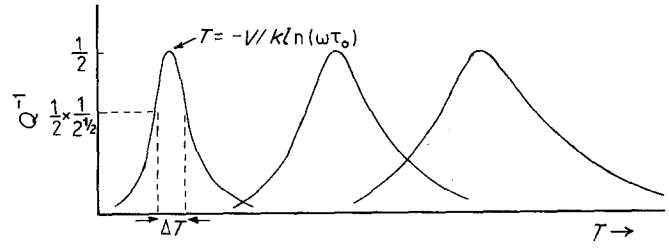

Figure 18 Illustrating the overlap on the temperature axis of a number of SLSLD processes of different relaxation time.

small ring. Further, angles more acute than the average are just as possible in a large ring as in small rings, given that they will be compensated by other angles straighter than average in the same ring. So we expect both the number of distorted (elongated/contracted) cation–cation spacings and the average degree of elongation and contraction to increase with average ring size. Thus we propose that both the number of two-well (acoustic) loss centres, and their average activation energy (i.e. the total area under, as well as the spread of the $n(V)$ against V spectrum), will increase with ring size.

8.3. Effect of bond strength (stretching force constant)

A second factor affecting the form of the two-well potentials in glass will be the cation–anion bond strengths. For a given A–O–A bond angle and A–A separation, inspection of our expresions for the potential in which the O atom moves (Equations 14 to 19) show that the barrier height will be directly proportional to the bond strength (i.e. to the bond-stretching force constant).

We now postulate that this is the only way in which the bond strength affects the two-well system, i.e. we assume that, for a given ring size, variations in bond strength do not affect the total number of distorted cation–cation spacings (loss centres) or the degree of distortion. At first sight the postulate can be criticized on the ground that as the A–O–A bond force constant increases, so also does the energy required to produce a given degree of bond angle or length distortion. However, against this it should be remembered that we do not have to account for this energy provision which is simply the excess energy associated with the amorphous state and is available during the process of glass formation. This postulate is required to provide an explanation of why the compositional dependence of $\int n(V)\,dV$ (and total number of loss centres) is strikingly different from that of the average activation energy.

In summary of Sections 8.1 to 8.3 we will attempt an interpretation of our own acoustic loss data, as well as data on other oxide glass forming systems given in the literature on the criteria.

(i) Both $\int n(V)\,dV$, and the total number of loss centres are proportional to oxygen density.

(ii) $\int n(V)\,dV$, total number of loss centres, and the average activation energy $\bar{V}$ all increase with atomic ring size.

(iii) For a given atomic ring size, $\bar{V}$ also increases with bond-strength or stretching force constant.

The possible extreme shapes of $n(V)$ against $\bar{V}$ curves based on the permutation of the variables in (i) and (ii) are sketched in Fig. 19.

It should be mentioned that, although there is a rough one-to-one correspondence, $\bar{V}$ defined as an arithmetical average over the relaxation spectrum, i.e. $\int Vc(V)\,dV/\int c(V)\,dV$, does not always agree with the average value determined from the peak-temperature frequency shift. With this in mind we take Rules (ii) and (iii) above to apply no matter how the average activation energy has been defined. However for simplicity, and as it is subject to the least computational error, during the rest of this paper we discuss only the average energy determined from the peak loss, denoted by V_p. The possible explanation of the discrepancy between differently defined average activation energies will be dealt with elsewhere.

8.4. Application of the model to the interpretation of the compositional dependence of the low-temperature acoustic loss of Mo–P–O glasses

By inspection of Figs 15 and 16, we note that the height of the loss peaks is fairly accurately proportional to $C(V)\,dV$ and the total number of loss centres. All these quantities vary in a similar manner with MoO_3 (mol %) and display the same discontinuities in composition gradient at about 53 and 66 mol % that we have found in the other physical properties of these glasses. In contrast, the average activation energy, V_p, and the (directly related) peak temperature are both monotonically decreasing functions of MoO_3 (mol %), displaying no evidence of discontinuities (Fig. 20), although the V_p curve displays a clear inflexion at 53 mol %.

For our interpretation we have adopted a qualitative model of the structure of Mo–P–O glass whose details are presented elsewhere [13, 14, 17] and can be summarized as follows.

(a) The oxygen density of the glass system exhibits a single pronounced minimum at 53 mol % MoO_3 content, the swing from maximum to minimum being about 6% (Patel and Bridge [13]).

(b) As MoO_3 content is increased gradually, the atomic ring size decreased to a minimum at 53 mol % as P_6O_6 (P_2O_5 oxide) rings are replaced by $Mo_2P_2O_3$ (metaphosphate) and $Mo_2P_2O_4$ (orthophosphate)

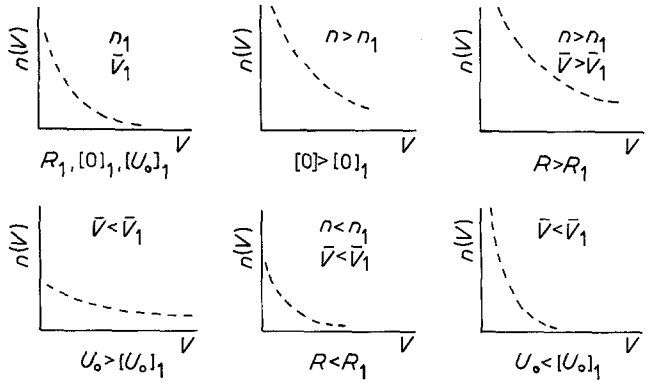

Figure 19 Schematic illustration of possible extreme shapes of $n(V)$ against $\bar{V}$ curves. Note that for constant speed c, the $n(V)-V$ curves are to scale with the $C(V)-V$ curves. Independent variables: R = ring size, [O] = oxygen density, U_0 = binding energy. Dependent variables: $n = \int_0^\infty n(V)\,dV$, $\bar{V} = \int_0^\infty Vn(V)\,dV$. These variables remain constant (R_1, $[O_1]$, $[U_0]_1$, n_1 and V_1, respectively) unless otherwise stated.

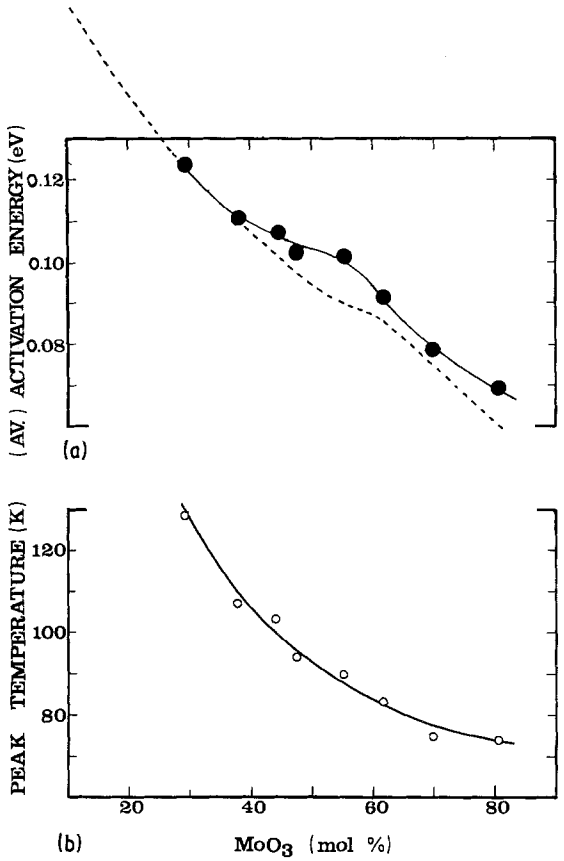

Figure 20 Compositional dependence of (a) the average activation energy, V_p, and (b) the peak temperature (P_h) at 44 MHz occurring in the low-temperature loss in molybdenum–phosphate glasses. The solid line is drawn through experimental data points and the dotted line is the theoretical curve predicted by Equation 39.

rings. At higher molybdenum contents the ring size increases again as the mix of *meta-* and *ortho-*phosphate rings are replaced by $Mo_2P_2O_4$ (pyrophosphate) rings. A maximum is reached at the pyrophosphate composition of 66 mol %, though the ring size is still substantially less than the sizes in the low molybdenum content glasses. Finally, further increases in molybdenum content lead to a further decrease in ring size as Mo_2O_2 (MoO_3 oxide) rings replace pyrophosphate rings. Overall the average ring size of the molybdenum-rich glasses (dominated by Mo_2O rings) is substantially less than that in the phosphorus-rich glasses (dominated by P_6O_6 rings) [14].

(c) There are several kinds of Mo–O and P–O bonds in the Mo–P–O glass. However, in all cases the Mo–O force constants are only one half of the values of P–O force constants [16]. Thus increasing the MoO_3 content from 0 to 83 mol % gradually decreases the average stretching force constant in the glass to about one half the starting value.

Examining Rules (i), (ii) and (iii) in the light of (a), (b) and (c) above, the general form of the compositional dependence of n and V_p is readily understood. Thus V_p evidently follows predominantly the trend of the force constant. On the other hand, unaffected by the force constant, variations of n follow substantially the form of the ring size variations described in (b). The oxygen density variations will sharpen the minimum in these quantities at about 53 mol % MoO_3, but will flatten the maximum at about 63 mol % MoO_3. However, oxygen density is of secondary importance compared with the ring size effect, given that the density changes by only 6% in the range 30 to 53 mol % whilst $\int c(V)\,dV$ and n have changed by 30 and 50%, respectively. Ring sizes themselves do not change by anything like this amount, but whereas only a linear dependence of n on oxygen density is plausible, a power-law dependence on ring size is admissable [15].

8.5. Application of the model to explain the different levels of average activation energy in glass systems based on different oxide glass formers

Quantitatively our criteria suggest empirical relationships of the form

$$N = \text{const}_1\, R^m \tag{30}$$

$$V_p = \text{const}_2\, f\, R^m \tag{31}$$

N is the number of loss centres expressed as a percentage of the number of oxygen atoms per unit volume, R is an average ring size and f is a mean stretching force constant for a given glass. If we are to test these equations, estimates of R and f for every glass will have to be made. Bridge *et al.* [16] argued that for pure inorganic oxide glasses quite reliable estimates of average ring sizes could be obtained from a consideration of the known structures of crystalline analogues. Further they argued that these ring sizes fitted the relationship

$$K = \text{const}_3\, f/R^n \tag{32}$$

where K is the bulk modulus, and a correlation coefficient of 99% with

$$\text{const}_3 = 0.0106, \qquad n = 3.84 \tag{33}$$

with f in $\mathrm{N\,m^{-1}}$, R in nm and K in Gpa. We shall assume that this relationship exists for multicomponent oxide glasses (assumed to be three-dimensional networks) with the force content being averaged over many bond types and the ring size being an average over several types of ring (e.g. P_6O_6, Mo_2O_2, MoP_2O_3, $Mo_2P_2O_4$ in Mo–P–O glasses). Then eliminating R between Equations 30 to 32 we have

$$N = \text{const}_4 \left(\frac{f}{K}\right)^{m/n} \tag{34}$$

$$V_p = \text{const}_5 f \left(\frac{f}{K}\right)^{m/n} \tag{35}$$

Representing the Mo–P–O glasses by the mole fraction composition formula $x\mathrm{MoO_3}(1-x)\mathrm{P_2O_5}$ we take the average force constant to be

$$f = \frac{n_1 x f_{\mathrm{M-O}} + n_2(1-x) f_{\mathrm{P-O}}}{n_1 + n_2} \tag{36}$$

where n_1 is the number of Mo–O network bonds per formula unit in MoO_3, n_2 is the number of P–O network bonds per formula unit of P_2O_5, and $f_{\mathrm{M-O}}$ and $f_{\mathrm{P-O}}$ are the mean force constants for the respective types of network bond. Taking $f_{\mathrm{P-O}} = 450\,\mathrm{nm^{-1}}$, $f_{\mathrm{M-O}} = 214\,\mathrm{nm^{-1}}$, $n_1 = 5$ and $n_2 = 5$ [17] the force constants of the eight glasses are as listed in Table II.

TABLE II Empirical relations between low-temperature loss parameters of Mo–P–O glasses, force constant f and bulk modulus k

MoO_3 (mol %)	K (GPa)	f ($N m^{-1}$)	N (exp) (%)	N_{theor} (%)*	$V_{p\,exp}$ (eV)	$V_{p\,theor}$ (eV)†
0	25.3	450	3.43‡	3.09	0.145‡	0.163
29.2	26.1	381	3.02	2.76	0.123	0.123
37.5	26.9	362	2.76	2.63	0.111	0.112
44.2	28.0	346	2.52	2.50	0.107	0.102
47.4	28.7	338	2.32	2.44	0.102	0.097
55.0	29.5	320	2.18	2.32	0.102	0.087
61.6	27.2	304	2.05	2.37	0.091	0.085
69.5	29.4	286	2.27	2.18	0.079	0.074
80.8	32.0	259	2.13	1.96	0.069	0.060

*$N_{theor} = 0.589\,(f/K)^{0.576}$.
†$V_{p\,theor} = 6.92 \times 10^{-5} f(f/K)^{0.576}$.
‡Values obtained by extrapolation of experimental data on Mo–P–O glasses.

Taking also the corresponding bulk modulus values [14] and performing linear regression on $\ln N$ and f/K one obtains

$$N = 0.589\,(f/K)^{0.576} \quad (37)$$

with a correlation coefficient of 80%.

Linear regression performed on V_p and $f(f/K)^{0.576}$ yields a relationship

$$V_p = 5.87 \times 10^{-5} f(f/K)^{0.576} + 0.02\,\text{eV} \quad (38)$$

with a correlation coefficient of 98%. However, to obtain an empirical relation in the simpler proposed form of Equation 31 we determine the one unknown constant of this equation by fitting the latter to the experimental V_p value for the first member of the glass series (29% MoO_3 content). The result is

$$V_p = 6.92 \times 10^{-5} f(f/K)^{0.576} \quad \text{eV} \quad (39)$$

Apart from the correlation coefficients, however, the most important feature of Equations 37 and 39 is the fact that they predict correctly the general character of the compositional dependence of n and V_p (Table II, Figs 16 and 20). Thus both a minimum and a less pronounced maximum in n are predicted at roughly *meta-* and pyrophosphate compositions, respectively, although experimentally these turning points occurred at somewhat higher compositions. And in the case of V_p a slight inflexion is predicted around metaphosphate composition, as found experimentally (Fig. 20) though of rather lower MoO_3 content.

In computing f from Equation 36 one obvious error is that the rupture of P = O bonds to produce P–O–P, Mo–O–P bridging bonds, and the possible replacement of the M–O dangling bond (in MoO_3) by Mo–O–P and Mo–O–Mo bridging bonds, have been neglected. (However, these two effects tend to cancel.) Possibly, one way of allowing for them is [14, 16] to regard the glasses as mixtures of *meta-*, ortho- and pyrophosphate groups (in addition to MoO_3 and P_2O_5 groupings) in mole fractions which are determined by the mole fractions in the composition formula. So plausibly a more accurate estimate of f is to be obtained by averaging over all the bond types in these extended structural groupings. This has been done [18] but the method is laborious and is not presented here. Little material change to the preceding results is obtained and we conclude that the approach cannot be justified until low-temperature loss data on other glass series become available to put the preceding model to more stringent tests.

From inspection of Equations 34 and 35 it will be observed that f can in fact be eliminated to yield the relation

$$V_p = \text{const}_6\, N^{(1+n/m)} K \quad (40)$$

Linear regression performed on $\ln(V_p/K)$ and $\ln N$ yields the result

$$V_p = 1.02 \times 10^{-3} N^{1.374} K \quad (41)$$

with a correlation coefficient of 75%.

The above considerations suggest that K and f may be regarded as indicators of the size and shape of the low-temperature ultrasonic loss peaks in oxide glasses. The acquisition of further data on other glasses to test the proposed model seems well worth while. Although loss peaks for all the pure inorganic oxide glasses have been reported the model has not been applied to these data because, unfortunately, the "average activation energy" has not been defined consistently in the different cases and more than one figure has been quoted for the energy in some cases. In any event it is better to test the model in the manner of this paper, i.e. by monitoring the loss as a function of gradual composition changes, so that it is relative rather than absolute values of the loss parameters that are important. For this purpose work on a number of binary phosphate glass systems is in progress.

References

1. C. A. MAYNELL, G. A. SAUNDERS and S. SCHOLES, *J. Non-Cryst. Solids* **12** (1973) 271.
2. J. JÄCKLE, L. PICHE, W. ARNOLD and S. HUNKLINGER, *ibid.* **20** (1976) 365.
3. K. S. GILROY and W. A. PHILLIPS, *Phil. Mag. B.* **43** (1981) 735.
4. O. L. ANDERSON and H. E. BÖMMEL, *J. Amer. Ceram. Soc.* **38** (1955) 125.
5. R. E. STRAKNA and H. T. SAVAGE, *J. Appl. Phys.* **35** (1964) 1445.
6. C. A. MAYNELL and G. A. SAUNDERS, *Solid State Commun.* **11** (1972) 1345.
7. R. JANOSCHEK, in "The Hydrogen Bond", edited by P. Schuster, G. Zundel and S. Sandorfly (North-Holland, Amsterdam, 1976) p. 194.
8. W. P. KRAEMER and G. H. F. DIERCKSEN, *Chem. Phys. Lett.* **5** (1970) 463.
9. J. M. FARLEY and G. A. SAUNDERS, *J. Non-Cryst. Solids* **18** (1975) 417.
10. M. R. VUKEVICH, *ibid.* **11** (1972) 25.
11. R. E. STRAKNA, *Phys. Rev.* **123** (1961) 2020.
12. R. L. MOZZI and B. E. WARREN, *J. Appl. Crystallogr.* **2** (1969) 164.
13. N. D. PATEL and B. BRIDGE, *Phys. Chem. Glasses* **24** (1983) 130.
14. B. BRIDGE and N. D. PATEL, *J. Mater. Sci.* **21** (1986) 1187.
15. J. T. KRAUSE and C. R. KURKJIAN, *J. Amer. Ceram. Soc.* **49** (1966) 134 and **51** (1968) 226.
16. B. BRIDGE, N. D. PATEL and D. N. WATERS, *Phys. Status Solidi* **77** (1983) 655.
17. B. BRIDGE and A. A. HIGAZY, *Phys. Chem. Glasses* **27** (1986) 1.
18. A. A. HIGAZY, PhD thesis, Brunel University (1984).

Received 8 October
and accepted 6 December 1985